PERMAFROST AND PERIGLACIAL PROCESSES
Permafrost and Periglac. Process. (2015)
Published online in Wiley Online Library
(wileyonlinelibrary.com) DOI: 10.1002/ppp.1841

Noah Modelling of the Permafrost Distribution and Characteristics in the West Kunlun Area, Qinghai-Tibet Plateau, China

Hao Chen,[1,2] *Zhuotong Nan,*[1]* *Lin Zhao,*[1] *Yongjian Ding,*[1] *Ji Chen*[1] *and Qiangqiang Pang*[1]

[1] Cold and Arid Regions Environmental and Engineering Research Institute, Chinese Academy of Sciences, Lanzhou, People's Republic of China
[2] University of Chinese Academy of Sciences, College of Resources and Environment, Beijing, People's Republic of China

ABSTRACT

The Noah land surface model (LSM) can simulate well the hydrological and thermal processes of permafrost in the Qinghai-Tibet Plateau (QTP) and provides more permafrost metrics than those of statistical empirical models. The aim of this study was to develop a prototype for permafrost modelling by Noah and validate the model with field data. This was accomplished by modifying Noah, introducing a new thermal roughness scheme, a parameter calibration method and extending the simulation depth to allow for soil heterogeneity. The modified Noah LSM was validated using observations from the Tanggula meteorological station. Key permafrost metrics were simulated, including mean annual ground temperature (MAGT) at the depth of zero annual amplitude (DZAA), active layer thickness (ALT) and ground ice content of the West Kunlun area in the QTP. The permafrost distribution of the West Kunlun was mapped using the simulated MAGT and compared to a permafrost distribution map based on field observations. Data from ten boreholes were used for verification. The simulation error of the MAGT is less than 1.0 °C for eight boreholes, and the ALT simulations have relative errors of less than 25 per cent for seven boreholes. The Kappa coefficient for the two maps is 0.70. Permafrost characteristics including the distribution of different permafrost types, DZAA, ALT, MAGT and ground ice content in the West Kunlun are strongly influenced by altitude and the local environment. Such permafrost modelling can be extended to the rest of the QTP. Copyright © 2015 John Wiley & Sons, Ltd.

KEY WORDS: Noah land surface model; permafrost characteristics; permafrost distribution; Qinghai-Tibet Plateau

INTRODUCTION

The Qinghai-Tibet Plateau (QTP) is the highest plateau in western China, with an average elevation of over 4000 m asl. Permafrost in the QTP is estimated to exceed 1 million km^2 in area and is sensitive to climate change (Cheng and Jin, 2013). Modelling of permafrost properties is essential to evaluate the thermal state, distribution and characteristics of permafrost (Scherler *et al*., 2010; Weismuller *et al*., 2011). It is also useful in projecting the response of permafrost to climate change and assessing hazards resulting from permafrost degradation (Farbrot *et al*., 2013; Marmy *et al*., 2013).

Statistical empirical models have been traditionally adopted in modelling the permafrost distribution in the QTP. The commonly used models include the Gaussian model (X. Li and Cheng, 1999), the mean annual ground temperature (MAGT) model (Nan *et al*., 2005), the permafrost table temperature model (Q. B. Wu *et al*., 2000) and the probability distribution model (J. Li *et al*., 2009). Such models, being comparatively simple, cannot represent well the regional differences in permafrost distribution. The simulation resolution and accuracy also vary with local environmental factors. In contrast, process-based models such as land surface models (LSMs) have advantages in temporal and spatial modelling with their regionally adaptable process options and parameterisation schemes (Riseborough *et al*., 2008; Etzelmüller, 2013). Significant permafrost metrics including the MAGT at the depth of zero annual amplitude (DZAA), active layer thickness (ALT) and ground ice content can also be obtained and analysed through land surface modelling. In practice, LSMs have been widely applied in

*Correspondence to: Z. Nan, Cold and Arid Regions Environmental and Engineering Research, Chinese Academy of Sciences Institute, Lanzhou, 730000, People's Republic of China. E-mail: nztong@lzb.ac.cn

Received 17 April 2014
Revised 20 January 2015
Accepted 10 February 2015

simulations of shallow soil layers of permafrost (Schaefer *et al*., 2009; Subin *et al*., 2013). In many cases, simulations of permafrost sites with varying substrates on the QTP have been conducted by improving the parameterisation schemes of thermal roughness, surface energy partitioning, organic matter, soil heterogeneity and supercooled water in permafrost (Yang *et al*., 2005; Luo *et al*., 2009; Chen *et al*., 2010; Xiao *et al*., 2012; Zeng *et al*., 2012). Hydrological and thermal processes in permafrost are complex due to multiple influences from the surrounding environment, especially water-energy interactions related to soil properties and ground ice content (Romanovsky and Osterkamp, 2000; Hinkel *et al*., 2001; Hoelzle *et al*., 2001; Kane *et al*., 2001), which pose a challenge in parameterising the process-based modelling of permafrost.

Modelling of the permafrost distribution and characteristics in the QTP is especially difficult given the scarcity of available survey data. Guo *et al*. (2012) projected the permafrost distribution and its future changes in the QTP by coupling the Community Land Model with a regional climate model (RegCM3). The generated permafrost distribution map was compared with the *Map of Permafrost Distribution on the Qinghai-Xizang* (*Tibetan*) *Plateau* (S. X. Li and Cheng, 1996). However, available data were very limited in preparing S. X. Li and Cheng's map in 1996 and survey data in the western QTP were largely absent. The ongoing changes in permafrost in the QTP since 1996 thus cannot be included. Consequently, the results of Guo *et al*. (2012) cannot be verified in a meaningful way. Modelling of the current permafrost distribution and characteristics in the QTP, especially in the remote area of the western QTP, is imperative, and thus the motivation for this study.

The Noah LSM (Mitchell, 2005) is widely used with many weather and regional climate models such as the North America Land Data Assimilation System (Mitchell *et al*., 2004) and the Land Information System (Peters-Lidard *et al*., 2007). Many studies (e.g. Velde *et al*., 2009; Yang *et al*., 2009; Chen *et al*., 2011; Zeng *et al*., 2012) have confirmed that Noah can simulate well the hydrological and thermal processes of permafrost. This study uses Noah to model permafrost in the QTP, which is characterised by a thin snowpack, alpine meadow or alpine desert in land cover and substantial gravel in the ground soil profile. It has two objectives. First, the Noah LSM was modified with a new thermal roughness scheme, a parameter calibration method and extension of the simulation depth allowing for soil heterogeneity in order to reflect the unique hydrological and thermal conditions of the QTP (a continental climate with intense radiation, strong wind and a cold, dry atmosphere). The modified Noah was validated against observations from a standard meteorological station, Tanggula (TGL). Second, the permafrost characteristics and distribution of the 43.7×10^3 km^2 West Kunlun area in the arid western QTP were simulated with the modified Noah and compared to permafrost in the pan-Arctic and Qinghai-Tibet Highway/Railway areas. It is the first time that land surface modelling in the remote area of the western QTP has been verified with field observations. In 2009, the Investigation of Permafrost and its Environment over the QTP (Zhao, 2009) project set up a series of active layer observation systems and boreholes in the once-unexplored West Kunlun area of the QTP. The modelling was verified against borehole data and compared to a permafrost distribution map based on field observations. This study develops a prototype of permafrost modelling that can be extended to the rest of the QTP.

METHODS

Modifications of the Noah Model

Noah LSM.

Noah is a multi-layer LSM evolved from the one-dimensional Planetary Boundary Layer model (Ek and Mahrt, 1991; Ek *et al*., 2003). It has adopted the Penman potential evaporation approach (Mahrt and Ek, 1984), a simple water balance model (Schaake *et al*., 1996) and a snow-frozen ground process (Koren *et al*., 1999). Before simulation, soil temperature, unfrozen water content and soil moisture are assigned for each layer as initial conditions. Meteorological data are the input forcing data and are brought to equilibrium to eliminate the uncertainty of the initial conditions. Simulation parameters include soil thermal and hydraulic parameters, vegetation parameters and lower boundary conditions. Noah features a moderate number of parameters and less computational intensity than that of other commonly used LSMs. To determine the relative sensitivity of soil parameters in permafrost modelling of the QTP, single-factor sensitivity analysis was carried out and three sensitive soil parameters out of the prescribed ten soil parameters of Noah were identified, including the soil quartz content (QTZ), the soil pore distribution index of the Clapp-Hornberger soil hydraulic conductivity function (BB) (Clapp and Homberger, 1978) and the saturated soil conductivity (SATDK). Thus, only a small number of parameters including the sensitive soil parameters, vegetation types and lower boundary conditions of the model are tuned during the parameterisation process.

A New Thermal Roughness Scheme.

Thermal roughness Z_{0h} is an important parameter in the energy exchange between ground and atmosphere. Noah adopted Equations 1 and 2 to calculate Z_{0h} (Zilitinkevich, 1995):

$$Z_{0h} = Z_{0m} \times \exp\left(-1.0kCRe_*^{0.5}\right) \quad (1)$$

$$Re_* = Z_{0m}u_*/v \quad (2)$$

where Z_{0h} is the thermal roughness, Z_{0m} is the aerodynamic roughness, $C = 0.075$, $k = 0.4$, Re_* is the Reynolds number, u_* is the frictional velocity and v is the liquid viscosity. This original Noah model generally underestimates land surface temperatures in the daytime and overestimates

sensible heat flux in arid and semi-arid regions. Therefore, a new thermal roughness scheme is proposed as Equation 3 (Chen *et al*., 2010).

$$Z_{0h} = (70v/u_*)\times\exp\left(-7.2u_*^{0.5}|T_*|^{0.25}\right) \quad (3)$$

where T_* stands for the potential temperature. Simulation of the land surface temperature and sensible heat flux of four stations (two in the QTP) in the arid and semi-arid regions were improved by adopting Equation 3 in the Noah model (Chen *et al*., 2010).

Introduction of Soil Heterogeneity.

Noah divides the 2 m soil column into four layers with homogenous properties by default. We have extended the simulation depth to below 15 m to obtain key permafrost metrics. The different soil parameter settings for each layer reflect the soil heterogeneity.

Soil Parameter Calibration.

The soil layers are divided into three types: the surface layer, subsurface layer and bottom layer. Soil types can also be further divided into several sub-types. Layers in each type or sub-type are assigned the same parameters. As soil parameters in the QTP are unique and cannot be covered by the original Noah settings, soil parameters or parameter value ranges were set for each type according to the soil profile, the laboratory soil particle distribution analysis or the original value settings in the Noah soil parameters table (Mitchell, 2005).

A new parameter calibration method is proposed by minimising the cost function through optimising the sensitive parameters. The cost function Φ is defined as the error of the simulated target variables to the observed ones. Firstly, the sensitive parameters are initialised within the prescribed range of values. Then, the value of one parameter is changed by a fixed step and the other parameters remain unchanged. The optimum value of the parameter is determined when the cost function Φ reaches its minimum. Then, the parameter is replaced by the optimum value and the optimisation of the next parameter follows the same procedure. When all the optimum values for sensitivity parameters are determined, the final simulation results are computed with all the optimum sensitivity parameters.

Model Validation

Soil temperature and unfrozen water content data from the standard meteorological station TGL (91°56'E, 33°04'N, 5100 m asl, Figure 1a) in the QTP were used for validation. The station is underlain with permafrost and located in a cold alpine meadow (Yao *et al*., 2008). The mean annual air temperature is -4.9 °C and the annual precipitation is around 400 mm during the years of 2007 to 2010. Meteorological data from 1 April 2007 to 31 December 2010 are used as the forcing data. The new thermal roughness scheme and the initial conditions of 1 April 2007 are adopted in the simulation. The simulation depth is 15 m and the vegetation type is defined as 'sparse vegetation'. Sensitive soil parameters (QTZ, BB and SATDK) of 0–1 m soil layers are provided by the laboratory soil particle size distribution analysis and the empirical model of soil parameters based on soil texture (Saxton and Rawls, 2006). Table 1 shows the settings of the sensitive soil parameters. The soil parameters of the subsurface and bottom layers are determined by the parameter calibration method proposed in the Soil Parameter Calibration section. The cost function Φ is defined as the Nash-Sutcliffe model efficiency coefficients (NSEs) of the soil temperature and unfrozen water content simulation of layers two, five and twelve as the layers can represent the surface layers, subsurface layers and bottom layers, respectively, and have a better quality of observation data. The NSEs of temperature simulation for the shallow soil layers (above 2.45 m) are above 0.8; those of unfrozen water content are above 0.5 (Table 2). The simulation error of the MAGT for the bottom layers is within 0.2 °C. The time series curves of the above results indicate that the modified Noah model can simulate well the hydrological and thermal processes in the permafrost area of the QTP (Figure 2). The simulation of hydrological processes is less successful than that of thermal processes, especially when the soil layer deepens.

Modelling of the Permafrost Distribution and Characteristics of the West Kunlun

West Kunlun Area and Data.

The West Kunlun (78.8–81.5°E, 34.5–36.1°N) area covers an area of 43.7×10^3 km^2 that consists of alpine mountains, lacustrine basin deposits, alluvial plains and small hills. Glaciers and lakes cover an area of about 6.3×10^3 km^2. The West Kunlun area ranges in elevation from 2797 m asl to 6399 m asl, with vast expanses of permafrost. The mean annual air temperature is -6.3 °C and the mean annual precipitation is 20.6 mm at Tianshuihai (TSH) station (80.9°E, 35.3°N, 4840 m asl) from the years 1965 to 1970 (Zhou *et al*., 2000). The West Kunlun area is sparsely covered with alpine steppes, alpine meadows and desert steppes.

In 2011, a field observation project Investigation of Permafrost and its Environment over the QTP (Zhao, 2009) drilled 32 boreholes (8–20 m deep), examined 67 test pits, carried out 18 Ground-penetrating radar traverses and measured 63 vegetation quadrats in the West Kunlun area (Figure 1a).

The field observations were used to produce a permafrost distribution map with a resolution of 250 m × 250 m (Figure 3a, 3d). The map was compared to the permafrost distribution maps of the West Kunlun based on Noah modelling. The map was compiled according to the lower boundary of permafrost, which was calculated from the borehole data and classified by four slope aspects: 4650 m asl in the north, 4800 m asl in the south and 4700 m asl in the east and in the west (K. Li *et al*., 2012; Zhao *et al*., 2012). The ArcGIS Spatial Analyst, Environmental Systems Research Institute, Redlands, CA, USA was used in the compilation of the map based on field data. It is the traditional method to compile a permafrost distribution map of

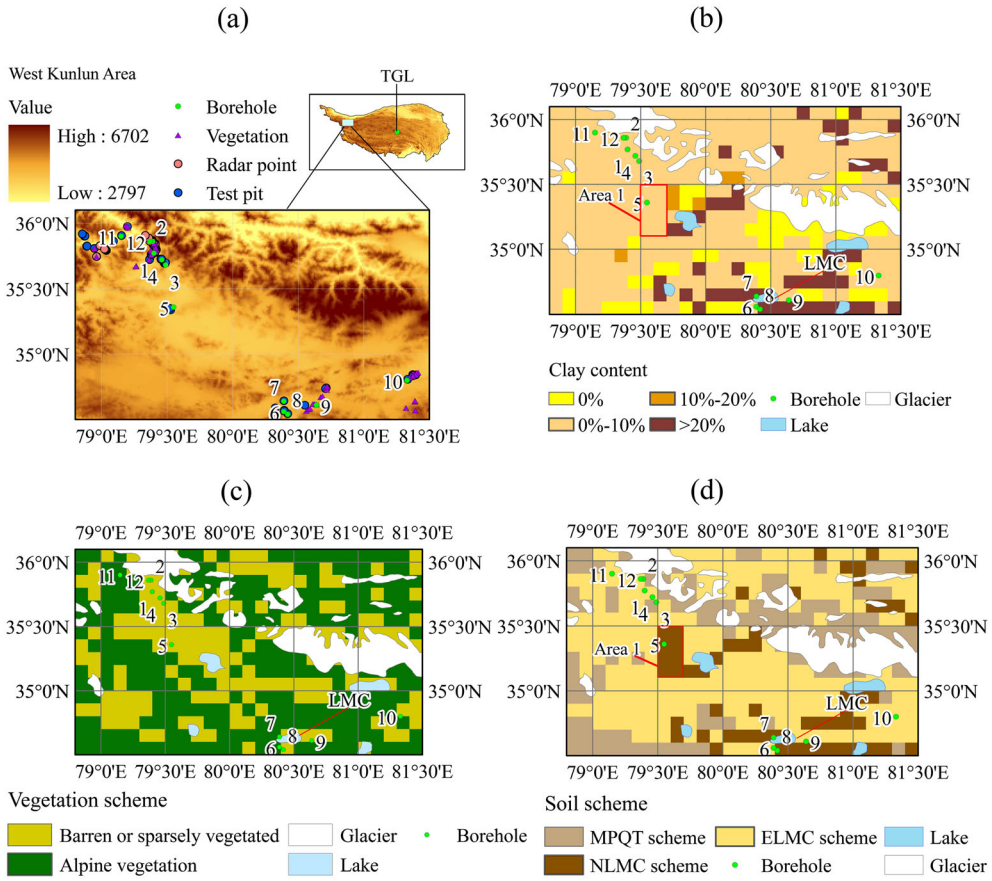

Figure 1 . (a) Map showing the locations of the TGL station and the West Kunlun area as well as the distribution of boreholes, vegetation plots, radar points and test pits over the West Kunlun area. Some sampling points overlap; (b) clay content distribution of the 0–1.2 m layer in the West Kunlun area; (c) distribution of vegetation schemes in the West Kunlun area; (d) distribution of soil schemes in the West Kunlun area. See text for abbreviations. This figure is available in colour online at wileyonlinelibrary.com/journal/ppp

Table 1 Soil layers and parameters at the TGL station.

Category	Number of layers	Depth(m)	QTZ	BB	SATDK × 10^{-6} m × s^{-1}	Soil description
Surface layer	2	0–0.12	0.65	4.52	4.12	Sandy loam
Subsurface layer 1	5	0.12–0.92	0.60	3.12	2.21	Sand, loam, gravel
Subsurface layer 2	6	0.92–3.02	[a]0.4–0.7	[b]2–5	[c]2–5	Sand, gravel
Bottom layer	10	3.02–15.82	[a]0.4–0.7	[b]2–5	[c]2–5	Sand, gravel, rock

[a]Value range of QTZ; [b]value range of BB; [c]value range of SATDK; value ranges of QTZ, BB and SATDK are determined by the field soil profile, the laboratory soil particle distribution analysis or the original value settings in the Noah soil parameters table. See text for abbreviations.

the QTP and the map has a higher resolution than the map based on Noah modelling.

A permafrost distribution map with a resolution of 0.1° × 0.1° (approximately 10 km × 10 km) was compiled according to the simulated value of the MAGT at the DZAA of each grid cell. Borehole whose altitude was closest to the average altitude of its grid cell was chosen to represent the thermal state and the soil parameter scheme of the grid cell. Geothermal data from the boreholes were used to verify the model. The locations, coordinates and altitudes of 12 representative boreholes are shown in Figure 1a and Table 3. Because the altitudes of boreholes No. 11 DYQK and No. 12 K508 are remarkably different from the average altitude of their grid cells, the thermal data of these boreholes were not used in verification but in establishing the linear regression equation for the lower boundary of modelling.

Ground Meteorological Forcing Data.

The meteorological forcing data-set used in this study is the China Meteorological Forcing Dataset (CMFD) (Chen *et al.*, 2011; He and Yang, 2011). The data-set has merged

Table 2 Nash-Sutcliffe model efficiency coefficients (NSEs) of soil temperature and unfrozen water content for the surface and subsurface layers and the simulated and observed MAGT of the bottom layers at the TGL station.

Category	Layer No.[a]	Depth (m)	NSE (soil temperature, °C)	NSE (unfrozen water content, %)	Simulated MAGT (°C)	Observed MAGT (°C)	Soil texture
Surface layer	2	0.05	0.955	0.653			Sandy loam
Surface layer	3	0.10	0.965	0.788			Sand, loam, gravel
Subsurface layer	5	0.40	0.966	0.521			Sand, loam, gravel
Subsurface layer	8	1.05	0.957	0.548			Sand, gravel
Subsurface layer	12	2.45	0.838	0.678			Water-saturated, gravel
Bottom layer	22	13	-0.341		-1.1	-1.3	Sand, gravel, rock
Bottom layer	23	15	-0.877		-1.1	-1.2	Sand, gravel, rock

[a]Number of layers counting down from the surface. See text for other abbreviations.

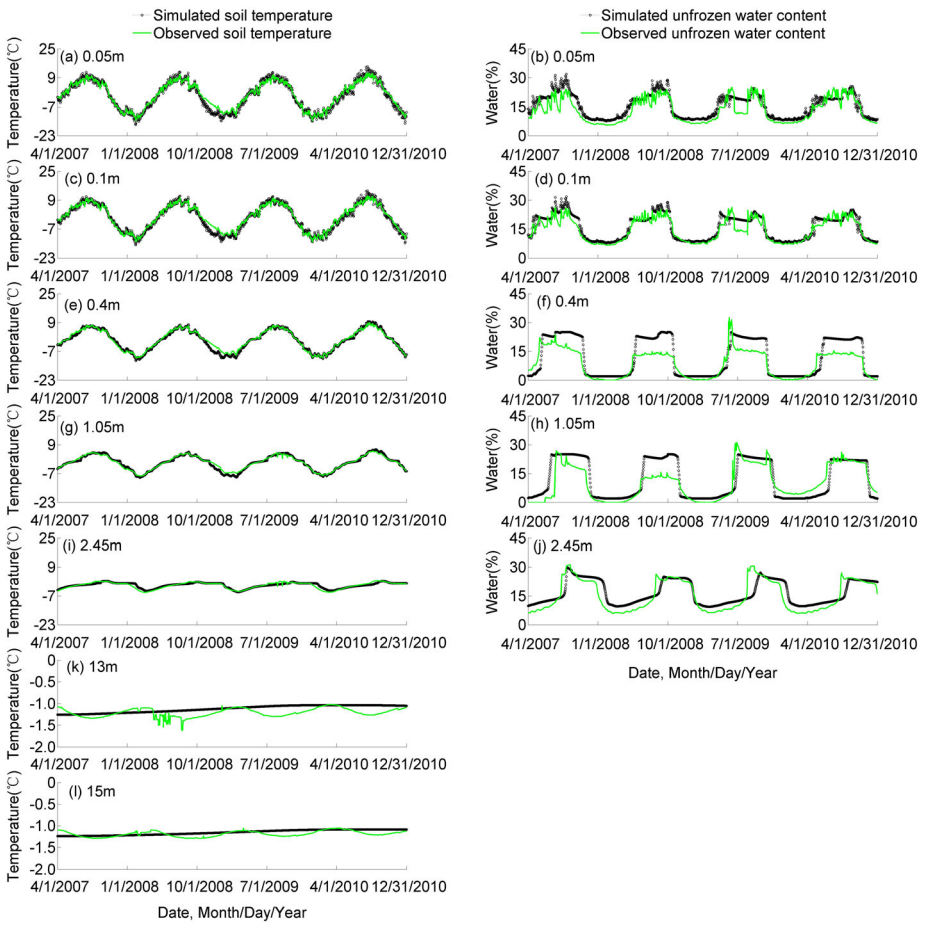

Figure 2 Simulated and observed unfrozen water content and soil temperature of the representative soil layers of the TGL station at different depths. See text for abbreviation. This figure is available in colour online at wileyonlinelibrary.com/journal/ppp

meteorological data from the China Meteorological Administration, reanalysis data-set of Princeton, Global Land Data Assimilation System, radiation data of Global Energy and Water Exchanges-Surface Radiation Budget and precipitation data of Tropical Rainfall Measuring Mission. The highest meteorological station involved in the CMFD is located in Anduo (91°5'E, 32°21'N) at 4800 m asl. The temporal resolution of the data is 3 h and the horizontal spatial resolution is 0.1°. The CMFD includes revisions of longwave and shortwave radiation errors of the QTP (Yang *et al.*, 2010) and has been successfully applied in permafrost and watershed hydrology simulations of the QTP (Guo and Wang, 2013; Xue *et al.*, 2013). The precipitation distribution of the CMFD in western China has been shown to be better than

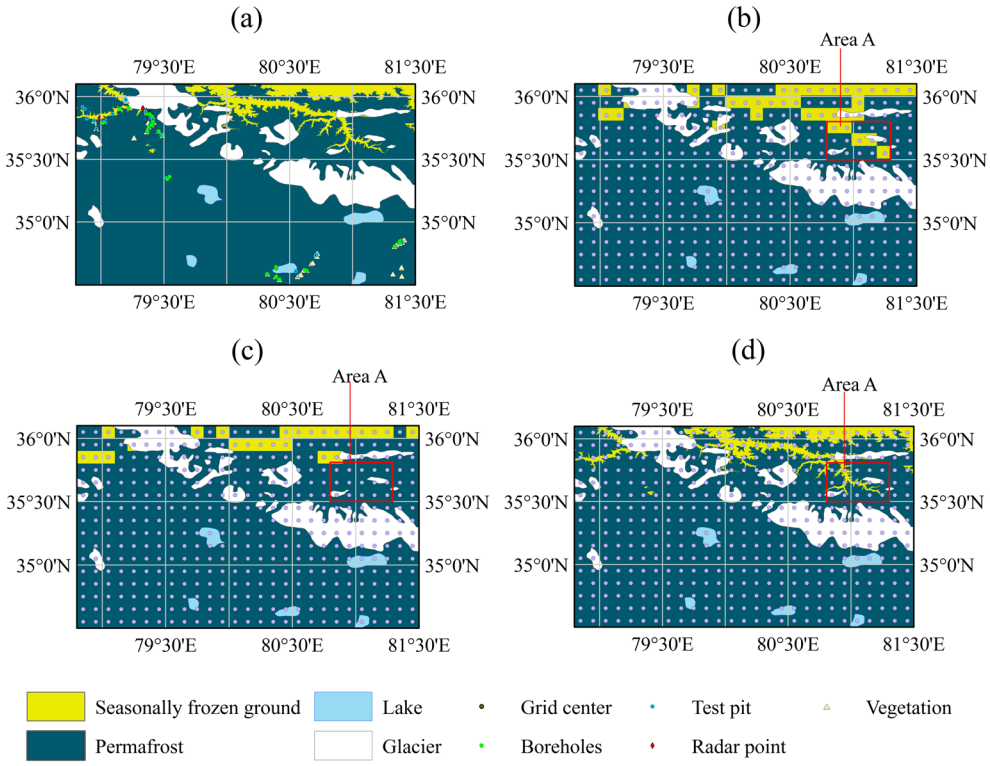

Figure 3 (a) Permafrost distribution map of the West Kunlun based on field observations with 250 m × 250 m resolution as well as the distribution of boreholes, vegetation plots, radar points and test pits; (b) permafrost distribution map of the West Kunlun based on field observations with 0.1° × 0.1° resolution; (c) simulated permafrost distribution map of the West Kunlun with 0.1° × 0.1° resolution; (d) permafrost distribution map of the West Kunlun based on field observations with 250 m × 250 m resolution as well as the distribution of the grid centers and Area A. This figure is available in colour online at wileyonlinelibrary.com/journal/ppp

Table 3 Location details of 12 boreholes and their corresponding grid cells in the West Kunlun.

ID	Code	Latitude (°)	Longitude (°)	Altitude (m)	Grid cell altitude (m)
1	YH	35.77	79.40	4850	4966
2	K512	35.86	79.39	4766	4848
3	MPQT	35.68	79.49	5175	5295
4	K529	35.72	79.46	4952	5018
5	TSH	35.36	79.55	4834	4839
6	SLMC	34.56	80.39	5050	5090
7	NLMC	34.64	80.39	5016	5069
8	MPJS	34.54	80.42	5177	5090
9	ELMC	34.61	80.64	5156	5148
10	LZL	34.80	81.33	5009	4986
11	DYQK	35.90	79.15	4319	5312
12	K508	35.86	79.37	4582	4848

See text for abbreviations.

that of other data-sets (Kan *et al.*, 2013). To verify the data quality, meteorological forcing data from 1 April 2007 to 31 December 2010 were extracted from the CMFD at the location of the TGL station. Pearson correlation analyses show that the daily air temperature of the CMFD and the TGL observation data is strongly correlated (r = 0.981, $p < 0.01$), as is the monthly precipitation data (r = 0.914, $p < 0.01$) (Figure 4), findings that are similar to previous studies (He, 2013; Kan *et al.*, 2013). Simulation results show that the NSE of the CMFD modelling of ground soil temperature (0.05 m) is above 0.9. Thus, the CMFD are suitable for the modelling of permafrost in the QTP.

Parameter Settings.

Three soil parameter schemes comprising a mountain pass in the Qitai area (MPQT), north of the Longmu Co

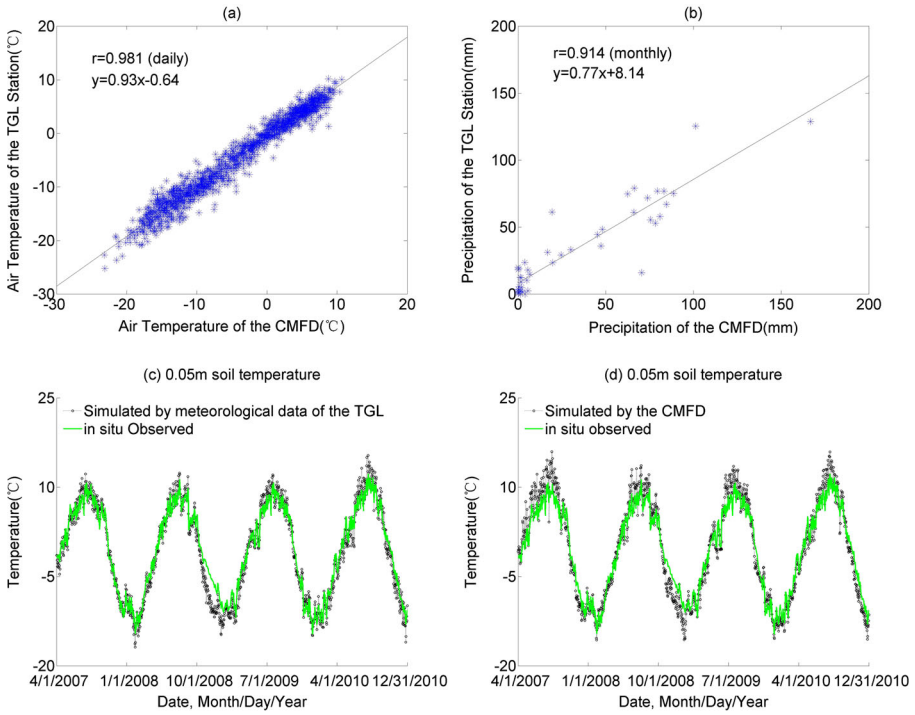

Figure 4 Linear regression curve of observation data from the TGL station and data extracted from the CMFD for (a) daily air temperature (linear regression equation y = 0.93x - 0.64; correlation coefficient r = 0.981) and (b) monthly precipitation (linear regression equation y = 0.77x + 8.14; correlation coefficient r = 0.914). Contrast of 0.05 m soil temperatures between *in-situ* observation and results simulated by the forcing data from (c) meteorological data of the TGL station and (d) CMFD at the TGL station. See text for abbreviations. This figure is available in colour online at wileyonlinelibrary.com/journal/ppp

Lake (NLMC) and east of the Longmu Co Lake (ELMC) were established using the soil profiles of the corresponding boreholes. The MPQT scheme is based on the soil profile of borehole No. 3 MPQT located in a high-altitude area. The soil surface is covered with gravelly soil, and bedrock occurs below a depth of 3 m. Grid cells with elevations exceeding 5295 m asl in the West Kunlun have adopted the MPQT scheme. The NLMC scheme is represented by borehole No. 7 NLMC located in a lacustrine deposit basin with high proportions of clay. Figure 1b shows the clay content of the West Kunlun extracted from the Harmonized World Soil Database (HWSD) (FAO/IIASA/ISRIC/ISS-CAS/JRC, 2009). Grid cells with clay content exceeding 20 per cent in the West Kunlun have adopted the NLMC scheme. The ELMC scheme is represented by borehole No. 9 ELMC located in an alluvial plain surrounded by hills with sandy and gravelly soil. The remaining grid cells in the West Kunlun have adopted the ELMC scheme. Table 4 shows the landscape, soil profiles, soil composition and stratification of different soil schemes in the West Kunlun. The distribution of the soil schemes is revised by borehole data. The TSH area (Area 1 in Figure 1b, d) was a lake since the Pleistocene period and gradually dried out, leaving substantial lacustrine deposits (B.Y. Li, 2000). Our field observations indicate that the deposits have high clay and ground ice contents, whereas the data from HWSD show that the clay content is less than 10 per cent. The field data are regarded as more reliable and

Table 4 Landscape, soil profiles, soil composition and stratification of the established three soil parameter schemes of the West Kunlun.

Soil parameter scheme	Landscape and landform	Surface layer (SL)	Subsurface layer (SSL)	Bottom layer (BL)	Stratification (SL:SSL:BL)[a]
MPQT	Mountain pass, barren land, southwest slope	Sand, loam, gravel	Sand, gravel	Gravel, rock	3:8:12
NLMC	Lacustrine deposit basin, plain, barren land	Sand, clay, loam	Clay, loam, gravel	Clay, sand, gravel	3:10:10
ELMC	Plain, barren land	Sand, loam	Sand, gravel	Sand, gravel	3:10:10

[a]Total soil layers of the SL, SSL and BL. See text for other abbreviations.

the TSH area adopts the NLMC scheme. The final distribution of the soil schemes can be seen in Figure 1d.

Sensitive soil parameters (QTZ, BB and SATDK) of the surface layer of the soil schemes were calculated from the soil particle size distribution analysis and the empirical model of soil parameters based on soil texture (Saxton and Rawls, 2006). The soil parameters of the subsurface and bottom layers were determined by the method proposed in the Soil Parameter Calibration section. The cost function Φ is defined as the error of simulated values of the MAGT at the DZAA compared to observations.

The deep soil temperature (DST) parameter was used as the lower boundary in the Noah LSM. In our case, soil temperature at 40 m was set as the DST. The DSTs of representative boreholes were calculated according to the geothermal gradient at 20 m depth. Then, the linear regression relationship between the DST and the altitude of the West Kunlun area was analysed using data from the 12 representative boreholes. The DST of borehole No. 5 TSH is abnormally low (Figure 5) because of its unique lacustrine deposits, and so it was excluded from analysis. The remaining 11 borehole DSTs were linearly fitted into a regression equation (Equation 4).

$$y = -0.0063x + 30.98 \tag{4}$$

where y is DST (°C) and x is altitude (m); the linear correlation coefficient r = -0.891. All of the grid cells except those in Area 1 were used to calculate the DST using Equation 4. All the grid cells in Area 1 adopted the DST of borehole TSH because they have similar altitudes, soil properties and environmental conditions.

The distribution of vegetation in the West Kunlun is derived from the 1:1 000 000 scale Vegetation Atlas of China (Chinese Editorial Board of Vegetation Map, 2001) and revised by the vegetation quadrats obtained through the field survey. According to the prescribed vegetation types of the Noah model, 'Barren or sparsely vegetated' and 'Alpine vegetation' are defined as two vegetation schemes in the West Kunlun. Figure 1c shows the vegetation scheme distribution in the West Kunlun.

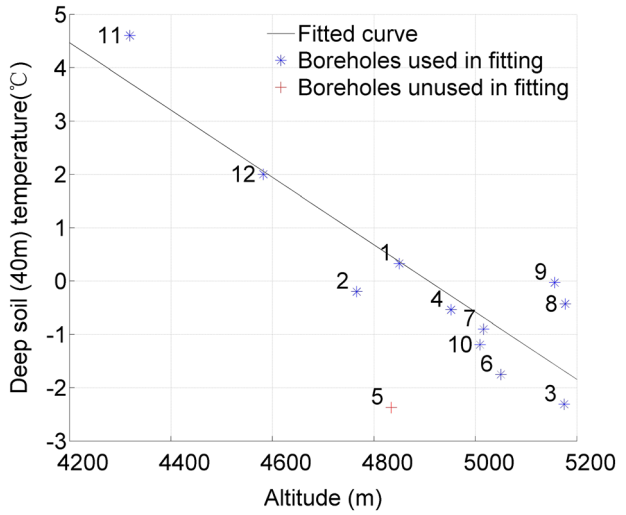

Figure 5 Linear regression curve of deep soil temperature (40 m) and altitude in the West Kunlun area (linear correlation coefficient r = -0.891). The curve is fitted by field temperature data from 11 representative boreholes at different altitudes. The temperature is used as the lower boundary of modelling in the West Kunlun area; borehole 5 is not used in fitting. This figure is available in colour online at wileyonlinelibrary.com/journal/ppp

Simulation of Permafrost Characteristics.

Forcing data between the years 2001 and 2010 were extracted from the CMFD and interpolated into 1 h time steps using MATLAB (MATLAB, The MathWorks, Natick, Massachusetts, USA) linear interpolation. A total of 432 grid cells of the West Kunlun were simulated with a resolution of 0.1° × 0.1° by the modified Noah LSM. The simulation depth was 18 m, deeper than the values of the DZAA of all grids. The initial conditions of representative boreholes were used for their grid cells. The initial conditions of boreholes MPQT, NLMC and ELMC were adopted as initial conditions for the remaining grid cells according to their soil parameter scheme (Figure 1d), except those in Area 1. The initial conditions of borehole No. 5 TSH were adopted for grids in Area 1 because they have higher ice contents compared to other areas that contain lacustrine deposits.

Previous studies have shown that the initial freezing date of the active layer in the QTP in the past 10 years is around mid-September, with variations of less than 10 days for stations ranging from 4400 m asl to 5100 m asl (Zhao *et al.*, 2000; R. Li *et al.*, 2012). The simulated ALT was set as the simulated maximum soil depth that remains above 0 °C during August, September and October of the last 3 years.

The ground ice content of the simulated depth was calculated by extracting the simulated soil moisture and unfrozen water content of the permafrost layer, and then calculating the total ground ice in each grid cell using Equations 5 and 6.

$$I = \sum_{i=1}^{n} \left(\left(\theta_i - \theta_i^{liquid} \right) \times V_i \times \frac{\rho_w}{\rho_{ice}} \right) \tag{5}$$

$$V_i = 10000 \times 10000 \times l_i \tag{6}$$

where I is the total ground ice content, i is the soil layer number i, n is the number of layers, θ_i is the volumetric soil moisture content of layer i, θ_i^{liquid} is the volumetric unfrozen water content of layer i, ρ_{ice} is the density of ice and set to $0.9 \times 10^3\,\mathrm{kg} \times \mathrm{m}^{-3}$, ρ_w is the density of water ($1.0 \times 10^3\,\mathrm{kg} \times \mathrm{m}^{-3}$), V_i is the volume of soil layer i (m^3) and l_i is the thickness of soil layer i (m).

RESULTS

Borehole Validation

The simulation errors of the MAGTs at the DZAA for eight of the ten simulated boreholes are within 1 °C and the

remaining two are within 1.5 °C (Table 5). The simulated MAGTs are generally lower than the observed ones, which can be attributed to the lower altitudes of boreholes compared to the average altitudes of simulated grid cells. However, since the altitude deviation is within 120 m, it is appropriate to verify the simulated thermal state of the grid cells with the borehole data. The observed MAGT of borehole No. 1 YH is 1.2 °C higher than that of the simulated one. To explain the large discrepancy, the general conditions of boreholes YH1, YH and the neighbouring borehole K512 were analysed. Field surveys showed that the area is scattered with salt lakes and that the thermal states of YH1 and YH are strongly influenced by the neighbouring salt lake. Boreholes nearer to the salt lakes tend to have higher MAGTs (Table 6), which is consistent with previous findings (Lin *et al*., 2010). In another case, borehole No. 7 NLMC is 350 m and borehole No. 6 SLMC is 1300 m from the Longmu Co Lake (LMC), an ancient glacial lake (Fontes *et al*., 1993). Field surveys have shown that the LMC can influence the ground temperature within 400–600 m. Boreholes nearer to the LMC have higher temperatures (Table 6). However, lakes of different areas and origins have different scales of influence on the thermal state of soil. Our results show that the simulation error for borehole NLMC is less than that of borehole YH. Borehole No. 3 MPQT is located in the sunny southwest aspect of an alpine pass. The influences of slope and aspect, which are not represented in the Noah model, together with other sources of uncertainty result in the simulation error of -1.4 °C.

MAGT Distribution

The MAGT at the DZAA shows a strong negative correlation with altitude ($r = -0.863$, $p < 0.01$) and a weak negative correlation with annual precipitation ($r = -0.327$, $p < 0.01$) (Table 7), which suggests that altitude controls permafrost distribution in the West Kunlun. The neighbouring Area 1 TSH and Area 2 have similar altitudes (Figure 6). Area 1 TSH belongs to the area of lacustrine deposits and adopts the NLMC scheme, whereas Area 2 adopts the ELMC scheme. Consequently, the MAGT of Area 1 is lower than that of Area 2 (Figure 6c), which reflects the influence of local ground features on the simulated MAGT. Similarly, the altitude of Area 3 is higher than that of Area 1 TSH, whereas surprisingly the MAGT of Area 3 is higher than that of Area 1 TSH. This can be attributed to the influence of different soil and vegetation types and to local geomorphic processes and topographically related climatic conditions. However, because Area 3 lacks borehole data, more field investigation is needed to explain the MAGT of Area 3.

Table 5 Simulated and observed values of MAGTs at the DZAA and ALT for the ten boreholes in the West Kunlun.

Code	ID	Simulated MAGT(°C)	Observed MAGT(°C)	[a]Error (°C)	Simulated ALT(m)	Observed ALT(m)	[a]Error (m)	[b]RE (%)
YH	1	-1.9	-0.7	-1.2	2.3	1.7	0.6	36.5
K512	2	-1.9	-1.1	-0.8	2.3	3.0	-0.7	22.7
MPQT	3	-4.2	-2.8	-1.4	1.6	2.5	-0.9	35.2
K529	4	-1.9	-1.7	-0.2	1.9	2.5	-0.6	24.8
TSH	5	-3.5	-3.0	-0.5	1.6	1.8	-0.2	10.0
SLMC	6	-2.7	-1.9	-0.8	2.3	2.8	-0.5	17.1
NLMC	7	-2.1	-1.8	-0.3	2.3	0.8	1.5	190.0
MPJS	8	-1.7	-1.3	-0.4	2.3	2.1	0.2	10.5
ELMC	9	-1.8	-1.3	-0.5	2.3	3.0	-0.7	22.7
LZL	10	-2.9	-2.3	-0.6	1.9	2.0	-0.1	5.0

[a]Difference between the simulated and observed metrics; [b]relative error of the ALT simulation. See text for abbreviations.

Table 6 Location details and site characteristics of six boreholes near the lakes.

Code	Location	Altitude (m)	MAGT (°C)	Distance to the lake (m)	Aspect	Slope
YH1	N:35.72, E:79.37	4780	-0.4	500	190	1°
YH	N:35.77, E:79.40	4850	-0.7	700	135	0.5°
K512	N:35.86, E:79.39	4766	-1.1	>1000	150	4°
NLMC1	N:35.64, E:80.39	5001	-0.9	200	0	0°
NLMC	N:35.64, E:80.39	5016	-1.8	350	150	4°
SLMC	N:34.56, E: 80.39	5050	-1.9	1300	0	0°

YH1, YH and K512 are near to the same salt lake; NLMC1, NLMC and SLMC are near to the Longmu Co Lake. See text for abbreviations.

Table 7 Correlation ($p < 0.01$) matrix of environmental parameters in the West Kunlun area.

	MAGT	Ground ice content	ALT
Altitude	-0.863	0.596	-0.499
Precipitation	-0.327	0.353	-0.540
MAGT	—	-0.576	0.771
ALT	0.771	-0.647	—

See text for abbreviations.

ALT Distribution

ALTs in the West Kunlun are mainly between 0 and 2.5 m (Figure 7b). The ALT shows weak negative correlations with altitude (r = -0.499, $p < 0.01$) and annual precipitation (r = -0.540, $p < 0.01$), and a strong positive correlation with the MAGT at the DZAA (r = 0.771, $p < 0.01$) (Table 7). This suggests that precipitation may be as crucial to the ALT as altitude, and that the ALT is closely related with soil temperature, such as the MAGT. The absolute value of ALT simulation errors of four boreholes of the ten simulated ones are more than 0.6 m and the largest one is 1.5 m (NLMC) (Table 5). Seven boreholes have relative errors of less than 25 per cent and two of less than 40 per cent, which is similar to previous modelling (Pang *et al.*, 2009). The large error in the NLMC borehole can be attributed to the freezing of the shallow soil layers as the borehole was drilled in early October. The inaccuracy of time-domain reflectometer measurement of the unfrozen water content in the active layer also contributes to the error. In general, the ALT simulation in this study is less accurate than the simulation of the MAGT but is regarded as acceptable.

Permafrost Classification and Distribution

Previous research suggests that the continuity-based permafrost classification proposed by the International Permafrost Association is not suitable for mountainous permafrost regions (Heginbottom, 2002). Our study adopted a MAGT-based permafrost classification focusing on the stability of high-altitude permafrost (Cheng, 1984), in which permafrost was classified as extremely stable, stable, sub-stable, transitional, unstable and extremely unstable according to the MAGT range at the DZAA. The altitudinal distribution of stable permafrost, sub-stable permafrost and transitional permafrost overlap, whereas seasonally frozen ground only occurs below 4300 m asl in river and mountain valleys (Table 8). High-altitude areas

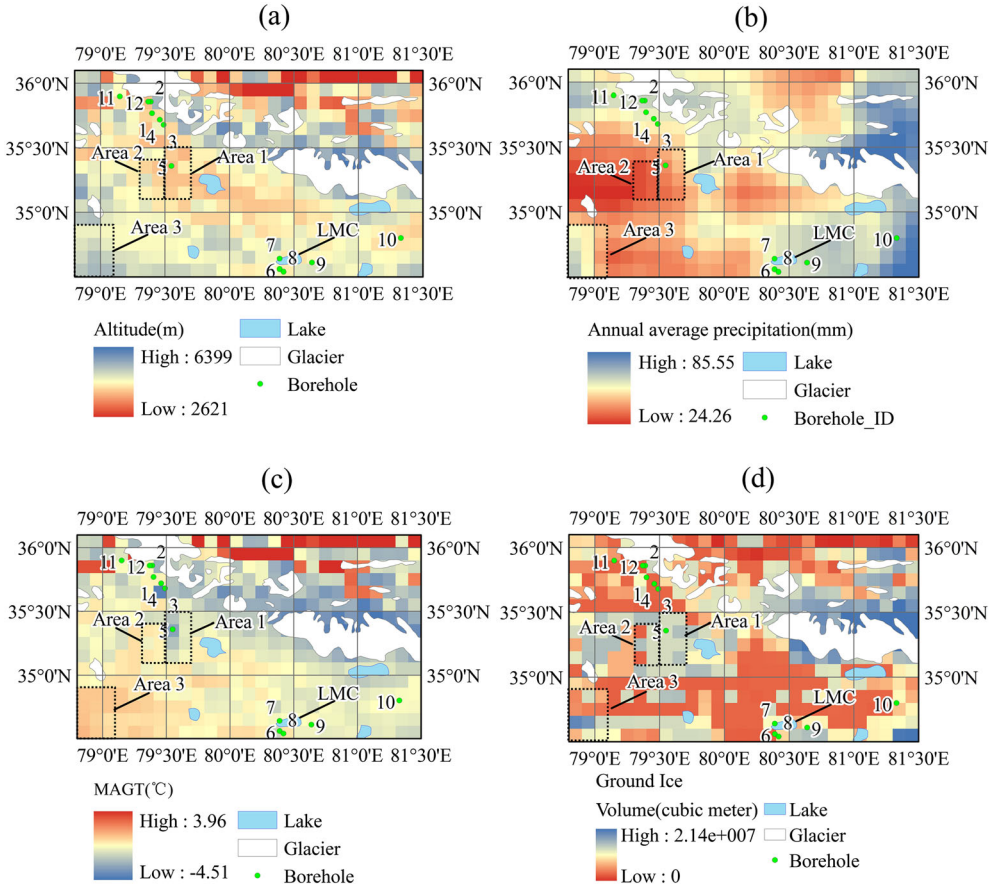

Figure 6 (a) Altitude and (b) annual average precipitation of the West Kunlun area; (c) simulated MAGT at the DZAA and (d) simulated ground ice content distribution in the West Kunlun area. See text for abbreviations. This figure is available in colour online at wileyonlinelibrary.com/journal/ppp

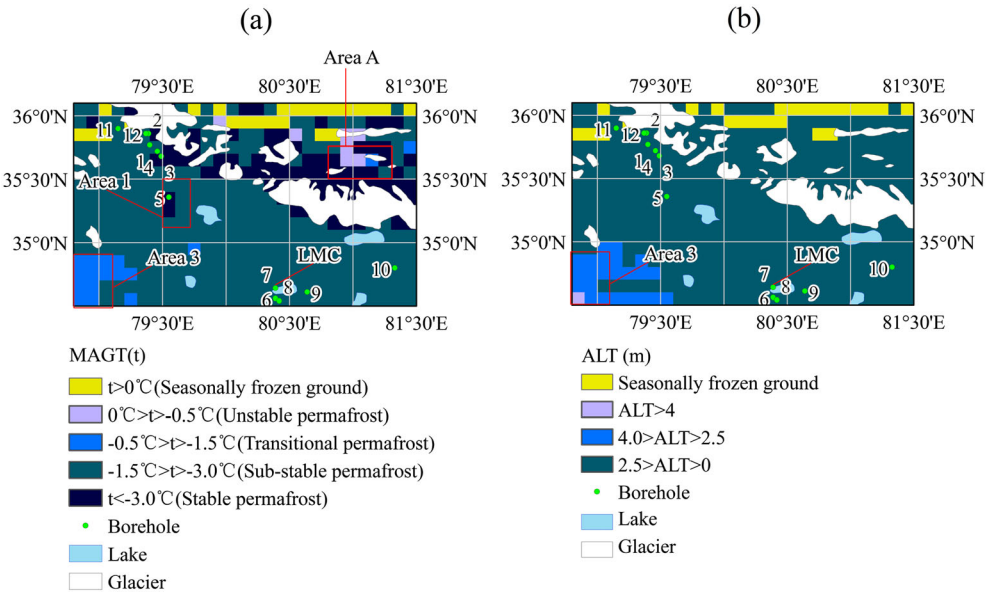

Figure 7 (a) Permafrost types based on the MAGT at the DZAA and the distribution of each type in the West Kunlun area; (b) ALT distribution map of the West Kunlun area with 0.1° × 0.1° resolution. See text for abbreviations. This figure is available in colour online at wileyonlinelibrary.com/journal/ppp

Table 8 Permafrost types (based on the MAGT at the DZAA) and altitude in the West Kunlun area.

Permafrost type	MAGT (°C)	Altitude (m)	Total grid cells
Extremely stable permafrost	< -5.0	—	
Stable permafrost	-3.0– -5.0	6399–4839	94
Sub-stable permafrost	-1.5– -3.0	5929-4767	290
Transitional permafrost	-0.5– -1.5	5742-4699	17
Unstable permafrost	0– -0.5	4703-4403	8
Seasonally frozen ground	>0	4329-2969	23

See text for abbreviations.

(above 5200 m asl) and lacustrine deposit areas (Area 1) tend to have stable permafrost (Figure 7a).

Ground Ice Content

The ground ice content within the simulated depth (15.82 m) was calculated using Equations 5 and 6. The ground ice content is positively correlated with altitude (r = 0.596, $p < 0.01$), negatively correlated with the MAGT distribution (r = -0.576, $p < 0.01$) and with the ALT (r = -0.647, $p < 0.01$), and weakly correlated with annual precipitation (r = 0.353, $p < 0.01$) (Table 7). The ice-rich permafrost is mainly distributed in the stable permafrost areas near glaciers and the lacustrine deposit Area 1 (Figure 6d). As no field data are available to verify the simulation of ice content, the results mainly suggest that the distribution trend in ground ice content has been influenced by meteorological factors during the past 10 years. More knowledge about the ancient climate of the West Kunlun since the late Pleistocene is needed to determine the accurate distribution of ground ice content.

Permafrost Distribution Map

The permafrost distribution map based on field observations at 250 m × 250 m resolution (Figure 3d) was upscaled to a resolution of 0.1° × 0.1° (Figure 3b). Using 0 °C of the MAGT at the DZAA to distinguish between permafrost and seasonally frozen ground, the simulated permafrost distribution map is shown in Figure 3c. Comparisons of Figure 3b–d show that the discrepancy between the maps of model data and observational data mainly occurs in the unstable permafrost areas, such as Area A, where the MAGT at the DZAA is above -0.5 °C. This is reasonable because the modelling accuracy of the MAGT at the DZAA is generally within 1 °C. Both maps were projected by the Albers projection to calculate the proportion of permafrost in the whole West Kunlun area without glaciers and lakes. Our results show that the area of simulated permafrost distribution is 35.0 × 10^3 km^2, accounting for 80.1 per cent of the West Kunlun area, and the area of simulated seasonally frozen ground is 2.4 × 10^3 km^2, accounting for 5.5 per cent (Figure 3c). For comparison, the area of observed

permafrost is 34.8×10^3 km^2, accounting for 79.7 per cent of the West Kunlun area, and the area of observed seasonally frozen ground is 2.6×10^3 km^2, accounting for 5.9 per cent (Figure 3d). The discrepancy of permafrost distribution in the two maps is 0.40 per cent. The Kappa coefficient for Figure 3b and c is 0.70, which indicates that the two maps substantially agree with each other.

DISCUSSION

Model Validation

Because fieldwork in the unexplored West Kunlun area is challenging and has begun only recently, no long-term data are available for model validation. The borehole data used are from *in-situ* observations collected during 3 months, and so the validation of soil temperatures is conducted with the MAGT at the DZAA. Previous work indicates that the DZAA on the QTP ranged from 10 to 15 m (Q. B. Wu *et al.*, 2010), whereas our simulations and measurements showed that the DZAA in West Kunlun ranged from 13 m to 17 m. Thus, we used geothermal data at the DZAA from ten boreholes ranging from 13 m to 17 m for model validation. Our results show that the model simulates well the values of the MAGT at the DZAA.

The soil in the QTP is generally rich in gravel and sand, which makes it difficult to determine the soil thermal and hydrological parameters when the simulated soil becomes deeper than 1 m and soil layers become thicker than 0.4 m. Thus, a soil parameter calibration method was applied to determine the soil parameters of the subsurface and bottom layers. The value ranges of soil parameters shown in Table 1 are determined by the field soil profile, the laboratory soil particle distribution analysis or the original value settings in the Noah soil parameters table. Our results show that the method is reasonable, although it is a coarse approach and more soil samples need to be acquired and analysed to verify the calibrated soil parameters.

Scaling Problems

The model resolution in this study is determined by the CMFD forcing data-set (0.1° × 0.1°). As the radiation and precipitation of the QTP are optimised in the CMFD, it is more reliable than other finer-scale data-sets for applications on the QTP (Guo and Wang, 2013; Xue *et al.*, 2013). However, many permafrost maps that are based on observations are at a resolution below 200 m × 200 m. As a result, downscaling or upscaling is needed to make comparisons between the maps, and both types of scaling introduce scaling error.

In our case, Area A in Figure 3d is located in the transitional area of unstable permafrost and seasonally frozen ground. After the 250 m × 250 m permafrost map (Figure 3d) is upscaled to 0.1° × 0.1° (Figure 3b), Figure 3b designates part of Area A as seasonally frozen ground, whereas the simulated 0.1° × 0.1° map (Figure 3c) designates Area A as complete permafrost. Such scaling operations can enlarge or shrink the proportion of permafrost and result in error in the comparison. Thus, the interpolation of forcing data should be considered carefully in order to create finer simulation maps. However, when the LSM simulation is near a resolution of 1 km × 1 km, lateral thermal flux and other environmental factors need to be considered, which requires further modifications of the models.

When borehole data are used to validate simulated geothermal conditions, the representativeness of boreholes to the corresponding grid cell should be carefully considered. Altitude, microclimate, surface characteristics, soil properties and the lower boundary of modelling are major factors that influence the permafrost distribution. Thus, the selected boreholes should occur in the general environment described by the above mentioned factors. Boreholes strongly influenced by other environmental factors such as rivers, lakes, hillslopes and aspect should be reconsidered.

Permafrost Characteristics of the West Kunlun Area

Other research in pan-Arctic permafrost areas demonstrates that the DZAA in sediments of discontinuous permafrost areas generally does not exceed 7 to 8 m, with the MAGT ranging from -1 to -3 °C (Romanovsky *et al.*, 2010; Smith *et al.*, 2010; Lewkowicz *et al.*, 2012). Boreholes in bedrock or bedrock overlain by metres of sediments in Scandinavia demonstrate that DZAAs can reach 10 to 16 m when MAGTs range from 0 to -4 °C, which can be ascribed to higher thermal diffusivities in the bedrock (Christiansen *et al.*, 2010; Farbrot *et al.*, 2011, 2013; Isaksen *et al.*, 2011). Boreholes along the Qinghai-Tibet Highway/Railway show that permafrost temperatures at 15 m depth (DZAA) are higher than -4.0 °C (Q. B. Wu *et al.*, 2010). Field observations indicate that permafrost areas developed in bedrock are small in the West Kunlun area. Our simulation shows that the DZAA in sediments of the permafrost area in the West Kunlun area ranges from 13 to 15 m, with the MAGT ranging from 0 to -4.5 °C. With the same MAGT, permafrost developed within sediments in the West Kunlun generally has a deeper DZAA compared with permafrost within sediments in higher latitudes. As the West Kunlun belongs to the semi-desert and alpine region, the phenomenon can be attributed to the scarcity of the snowpack, the richness of gravel and sand in soil, and the sparsely vegetated land cover. The thermal state of permafrost in the West Kunlun is in accordance with permafrost along the Qinghai-Tibet Highway/Railway with respect to the DZAA and MAGT (Q. B. Wu *et al.*, 2010).

Our simulation results show that the West Kunlun belongs to the predominantly plateau discontinuous permafrost region, with small areas of seasonal frost distributed in river and mountain valleys (Figure 7a). The permafrost types mainly include stable and sub-stable permafrost. The conclusion is in accordance with the map of the distribution of frozen ground in China (Ran *et al.*, 2012) and different from the map of geocryological regionalisation and

classification in China, in which the West Kunlun is defined as a predominantly continuous permafrost region (Qiu *et al*., 2000). During the past 20 to 30 years, borehole data show that the ground surface temperature has increased by 0.60 °C decade^{-1} in the QTP (T. Wu *et al*., 2013). Field observations in the TSH area of the West Kunlun show evidence of permafrost degradation with large-scale degraded vegetation and soil salinisation (Yu *et al*., 2006). Our field observations and modelling support the view that current permafrost in the West Kunlun is predominantly plateau discontinuous permafrost. Whether or not it is related with ongoing permafrost degradation still needs further investigation.

CONCLUSIONS

Our study draws the following conclusions:

1. The Noah LSM has been modified to meet the requirements of permafrost modelling of the QTP by introducing a new thermal roughness scheme, a soil parameter calibration method and by extending the simulation depth to allow for soil heterogeneity. It is the first time that land surface modelling in the remote western QTP is fully validated with field data. Although our results show that the modelling is sound, the modelling accuracy and resolution still need improvements. Error control in downscaling or upscaling of simulation is necessary, and more field observations of the key environmental factors such as soil texture are needed. Our modelling provides a prototype that can be extended to the rest of the QTP.
2. The Noah LSM can simulate the temporal and spatial distribution of permafrost metrics such as the MAGT, ALT, DZAA and the ground ice content. Noah can represent the comprehensive influence of environmental factors on permafrost, making it suitable for research investigating permafrost evolution under conditions of climate change.
3. The thermal state of permafrost in the West Kunlun is similar to permafrost along the Qinghai-Tibet High way/Railway with respect to the DZAA and the MAGT, and slightly different from permafrost in pan-Arctic areas. The type of permafrost in the West Kunlun is predominantly plateau discontinuous permafrost, and it is strongly influenced by local environmental factors.

ACKNOWLEDGEMENTS

The authors would like to thank financial support from the National Major Scientific Project of China (2013CBA01803), the National Science Foundation of China (41471059), the State Key Laboratory Open Foundation (SKLFSE201009) and the Hundred Talents Program of the Chinese Academy of Sciences (51Y251571). Ground based datasets for model calibration and validation were provided by the research group of "Investigation on permafrost and its environments on the Tibetan Plateau (2008FY110200)". Vegetation, soil, glacier and lake data-sets are from the Environment and Ecological Science Data Center for West China: http://westdc.westgis.ac.cn. Professor William Gough of the University of Toronto Scarborough assisted with the editing of the manuscript.

REFERENCES

Chen YY, Yang K, Zhou DG, Qin J, Guo XF. 2010. Improving the Noah land surface model in arid regions with an appropriate parameterization of the thermal roughness length. *Journal of Hydrometeorology* **11**: 995–1006. DOI:10.1175/2010JHM1185.1.

Chen YY, Yang K, He J, Qin J, Shi JC, Du JY, He Q. 2011. Improving land surface temperature modeling for dry land of China. *Journal of Geophysical Research* **116**: D20104. DOI: 10.1029/2011JD015921

Cheng GD. 1984. Problems on zonation of high-altitude permafrost. *Acta Geographica Sinica* **39**: 185–193 (in Chinese with English abstract).

Cheng GD, Jin HJ. 2013. Permafrost and groundwater on the Qinghai-Tibet Plateau and in northeast China. *Hydrogeology Journal* **21**: 5–23. DOI:10.1007/s10040-012-0927-2.

Chinese Editorial Board of Vegetation Map. 2001. *Vegetation Atlas of China (1:1 000 000)*. Science Press: Beijing, China (in Chinese).

Christiansen HH et al. 2010. The Thermal State of Permafrost in the Nordic Area during the International Polar Year 2007-2009. *Permafrost and Periglacial Processes* **21**: 156–181. DOI:10.1002/ppp.687.

Clapp RB, Homberger GM. 1978. Empirical equations for some soil hydraulic properties. *Water Resources Research* **14**: 601–604. DOI:10.1029/WR014i004p00601.

Ek MB, Mahrt L. 1991. OSU 1-D PBL Model User's Guide. 1–119.

Ek MB, Mitchell KE, Lin Y, Rogers E, Grunmann P, Koren V, Gayno G, Tarpley JD. 2003. Implementation of Noah land surface model advances in the National Centers for Environmental Prediction operational mesoscale Eta model. *Journal of Geophysical Research* **108**: 8851. DOI: 10.1029/2002JD003296.

Etzelmüller B. 2013. Recent Advances in Mountain Permafrost Research. *Permafrost and Periglacial Processes* **24**: 99–107. DOI:10.1002/ppp.1772.

FAO/IIASA/ISRIC/ISS-CAS/JRC. 2009. *Harmonized World Soil Database (version 1.1)*. FAO, Rome, Italy and IIASA, Laxenburg, Austria.

Farbrot H, Hipp TF, Etzelmüller B, Isaksen K, Ødegård RS, Schuler TV, Humlum O. 2011. Air and Ground Temperature Variations Observed along Elevation and Continentality Gradients in Southern Norway. *Permafrost and Periglacial Processes* **22**: 343–360. DOI:10.1002/ppp.733.

Farbrot H, Isaksen K, Etzelmüller B, Gisnås K. 2013. Ground Thermal Regime and Permafrost Distribution under a Changing Climate in Northern Norway. *Permafrost and Periglacial Processes* **24**: 20–38. DOI:10.1002/ppp.1763.

Fontes JC, Melieres F, Gibert E, Qing L, Gasse F. 1993. Stable isotope and radiocarbon balances of two Tibetan lakes (Sumxi Co, Longmu Co) from 13,000 BP. *Quaternary Science Reviews* **12**: 875–887.

Guo DL, Wang HJ. 2013. Simulation of permafrost and seasonally frozen ground conditions on the Tibetan Plateau, 1981–2010. *Journal of Geophysical Research-Atmospheres* **118**: 5216–5230. DOI:10.1002/jgrd.50457.

Guo DL, Wang HJ, Li D. 2012. A projection of permafrost degradation on the Tibetan Plateau during the 21st century. *Journal of*

Geophysical Research **117**: D05106. DOI: 10.1029/2011JD016545

He J, Yang K. 2011. China Meteorological Forcing Dataset (ed). Cold and Arid Regions Science Data Center at Lanzhou. DOI: 10.3972/westdc.002.2014.db

He SW. 2013. Meteorological forcing data evaluation and water heat processes simulation over the upstream area of the Heihe River Basin (in Chinese with English abstract), Master Dissertation, College of water resource and hydropower, Sichun University.

Heginbottom JA. 2002. Permafrost mapping: a review. *Progress in Physical Geography* **26**: 623–642. DOI:10.1191/0309133302pp355ra.

Hinkel KM, Paetzold F, Nelson FE, Bockheim JG. 2001. Patterns of soil temperature and moisture in the active layer and upper permafrost at Barrow, Alaska: 1993–1999. *Global and Planetary Change* **29**: 293–309. DOI: 10.1016/s0921-8181(01)00096-0.

Hoelzle M, Mittaz C, Etzelmüller B, Haeberli W. 2001. Surface energy fluxes and distribution models of permafrost in European mountain areas: an overview of current developments. *Permafrost and Periglacial Processes* **12**: 53–68. DOI: 10.1002/ppp385

Isaksen K, Ødegård RS, Etzelmüller B, Hilbich C, Hauck C, Farbrot H, Eiken T, Hygen HO, Hipp TF. 2011. Degrading Mountain Permafrost in Southern Norway: Spatial and Temporal Variability of Mean Ground Temperatures, 1999-2009. *Permafrost and Periglacial Processes* **22**: 361–377. DOI: 10.1002/ppp.728.

Kan BY, Su FG, Tong K, Zhang LL. 2013. Analysis of the Applicability of Four Precipitation Datasets in the Upper Reaches of the Yarkant River,the Karakorum. *Journal of Glaciology and Geocryology* **35**: 710–722 (in Chinese with English abstract).

Kane DL, Hinkel KM, Goering DJ, Hinzman LD, Outcalt SI. 2001. Non-conductive heat transfer associated with frozen soils. *Global and Planetary Change* **29**: 275–292. DOI: 10.1016/s0921-8181(01)00095-9.

Koren V, Schaake J, Mitchell K, Duan Q-Y, Chen F, Baker JM. 1999. A parameterization of snowpack and frozen ground intended for NCEP weather and climate models. *Journal of Geophysical Research* **104**: 19569–19585.

Lewkowicz AG, Bonnaventure PP, Smith SL, Kuntz Z. 2012. Spatial and thermal characteristics of mountain permafrost, northwest Cananda. *Geografiska Annaler Series a-Physical Geography* **94A**: 195–213. DOI: 10.1111/j.1468-0459.2012.00462.x.

Li BY. 2000. The last greatest lakes on the Xizang (Tibetan) Plateau. *Acta Geographica Sinica* **55**: 182–188 (in Chinese with English abstract).

Li SX, Cheng GD. 1996. *Map of Permafrost Distribution on the Qinghai -Xizang (Tibetan) Plateau, scale 1:3,000,000*. Gansu Cultural Press: Lanzhou, China (in Chinese).

Li X, Cheng GD. 1999. The response model of high altitude permafrost to global climate change. *Science in China (Series D)* **29**: 185–192.

Li J, Sheng Y, Wu JC, Chen J, Zhang XM. 2009. Probability distribution of permafrost along a transportation corridor in the northeastern Qinghai province of China. *Cold Regions Science and Technology* **59**: 12–18.

Li K, Chen J, Zhao L, Zhang X, Pang Q, Fang H, Liu G. 2012. Permafrost Distribution in Typical Area of West Kunlun Mountains Derived from a Comprehensive Survey. *Journal of Glaciology and Geocryology* **34**: 447–454 (in Chinese with English abstract).

Li R, Zhao L, Ding Y, Wu T, Xiao Y, Du E, Liu G, Qiao Y. 2012. Temporal and spatial variations of the active layer along the Qinghai-Tibet Highway in a permafrost region. *Chinese Science Bulletin* **57**: 4609–4616. DOI:10.1007/s11434-012-5323-8.

Lin ZJ, Niu FJ, Xu ZY, Xu J, Wang P. 2010. Thermal Regime of a Thermokarst Lake and its Influence on Permafrost, Beiluhe Basin, Qinghai-Tibet Plateau. *Permafrost and Periglacial Processes* **21**: 315–324. DOI:10.1002/ppp.692.

Luo SQ, Lü SH, Zhang Y. 2009. Development and validation of the frozen soil parameterization scheme in Common Land Model. *Cold Regions Science and Technology* **55**: 130–140. DOI:10.1016/j.coldregions.2008.07.009.

Mahrt L, Ek M. 1984. The influence of atmospheric stability on potential evaporation. *Journal of Climate and Applied Meteorology* **23**: 222–234.

Marmy A, Salzmann N, Scherler M, Hauck C. 2013. Permafrost model sensitivity to seasonal climatic changes and extreme events in mountainous regions. *Environmental Research Letters* **8**: 35–48. DOI:10.1088/1748-9326/8/3/035048.

Mitchell KE. 2005. *Noah LSM USERGUIDE 2.7.1*. National Centers for Environmental Prediction/Environmental Modeling Center. College Park: MD, USA.

Mitchell KE, Lohmann D, Houser PR, Wood EF, Schaake JC, Robock A, Cosgrove BA, Sheffield J, Duan QY, Luo LF, Higgins RW, Pinker RT, Tarpley JD, Lettenmaier DP, Marshall CH, Entin JK, Pan M, Shi W, Koren V, Meng J, Ramsay BH, Bailey AA. 2004. The multi-institution North American Land Data Assimilation System (NLDAS): Utilizing multiple GCIP products and partners in a continental distributed hydrological modeling system. *Journal of Geophysical Research-Atmospheres* **109**: D07S90. DOI:10.1029/2003jd003823.

Nan Z, Li S, Cheng G. 2005. Prediction of permafrost distribution on the Qinghai-Tibet Plateau in the next 50 and 100 years. *Science in China Series D* **48**: 797–804.

Pang Q, Cheng G, Li S, Zhang W. 2009. Active layer thickness calculation over the Qinghai-Tibet Plateau. *Cold Regions Science and Technology* **57**: 23–28. DOI:10.1016/j.coldregions.2009.01.005.

Peters-Lidard CD, Houser PR, Tian Y, Kumar SV, Geiger J, Olden S, Lighty L, Doty B, Dirmeyer P, Adams J. 2007. High-performance Earth system modeling with NASA/GSFC's Land Information System. *Innovations in Systems and Software Engineering* **3**: 157–165.

Qiu GQ, Zhou Y, Guo D, Wang Y. 2000. *The Map of Geocryological Regionalization and Classification in China*. Science Press: Beijing (in Chinese).

Ran Y, Li X, Cheng G, Zhang T, Wu Q, Jin H, Jin R. 2012. Distribution of Permafrost in China: An Overview of Existing Permafrost Maps. *Permafrost and Periglacial Processes* **23**: 322–333. DOI:10.1002/ppp.1756.

Riseborough D, Shiklomanov N, Etzelmüller B, Gruber S, Marchenko S. 2008. Recent advances in permafrost modelling. *Permafrost and Periglacial Processes* **19**: 137–156. DOI:10.1002/ppp.615.

Romanovsky VE, Osterkamp TE. 2000. Effects of unfrozen water on heat and mass transport processes in the active layer and permafrost. *Permafrost and Periglacial Processes* **11**: 219–239. DOI: 10.1002/1099-1530(200007/09)11:3<219::aid-ppp352>3.0.co;2-7

Romanovsky VE, Drozdov DS, Oberman NG, Malkova GV, Kholodov AL, Marchenko SS, Moskalenko NG, Sergeev DO, Ukraintseva NG, Abramov AA, Gilichinsky DA, Vasiliev AA. 2010. Thermal State of Permafrost in Russia. *Permafrost and Periglacial Processes* **21**: 136–155. DOI: 10.1002/ppp.683.

Saxton KE, Rawls WJ. 2006. Soil Water Characteristic Estimates by Texture and Organic Matter for Hydrologic Solutions. *Soil Science Society of America Journal* **70**: 1569–1578. DOI:10.2136/sssaj2005.0117.

Schaake JC, Koren VI, Duan QY, Mitchell K, Chen F. 1996. Simple water balance model for estimating runoff at different spatial and temporal scales. *Journal of Geophysical Research* **101**: 7461–7475. DOI:10.1029/95JD02892.

Schaefer K, Zhang TJ, Slater AG, Lu LX, Etringer A, Baker I. 2009. Improving

simulated soil temperatures and soil freeze/thaw at high-latitude regions in the Simple Biosphere/Carnegie-Ames-Stanford Approach model. *Journal of Geophysical Research-Earth Surface* **114**: F02021. DOI:10.1029/2008jf001125.

Scherler M, Hauck C, Hoelzle M, Stahli M, Volksch I. 2010. Meltwater Infiltration into the Frozen Active Layer at an Alpine Permafrost Site. *Permafrost and Periglacial Processes* **21**: 325–334. DOI:10.1002/ppp.694.

Smith SL, Romanovsky VE, Lewkowicz AG, Burn CR, Allard M, Clow GD, Yoshikawa K, Throop J. 2010. Thermal State of Permafrost in North America: A Contribution to the International Polar Year. *Permafrost and Periglacial Processes* **21**: 117–135. DOI:10.1002/ppp.690.

Subin ZM, Koven CD, Riley WJ, Torn MS, Lawrence DM, Swenson SC. 2013. Effects of Soil Moisture on the Responses of Soil Temperatures to Climate Change in Cold Regions. *Journal of Climate* **26**: 3139–3158. DOI:10.1175/jcli-d-12-00305.1.

Velde RVD, Su Z, Ek M, Rodell M, Ma Y. 2009. Influence of thermodynamic soil and vegetation parameterizations on the simulation of soil temperature states and surface fluxes by the Noah LSM over a Tibetan plateau site. *Hydrology and Earth System Sciences* **13**: 759–777.

Weismuller J, Wollschlager U, Boike J, Pan X, Yu Q, Roth K. 2011. Modeling the thermal dynamics of the active layer at two contrasting permafrost sites on Svalbard and on the Tibetan Plateau. *The Cryosphere* **5**: 741–757. DOI:10.5194/tc-5-741-2011.

Wu QB, Li X, Li WJ. 2000. Computer simulation and mapping of the regional distribution of permafrost along the Qinghai-Xizang Highway. *Journal of Glaciology and Geocryology* **22**: 323–326 (in Chinese with English abstract).

Wu QB, Zhang TJ, Liu YZ. 2010. Permafrost temperatures and thickness on the Qinghai-Tibet Plateau. *Global and Planetary Change* **72**: 32–38. DOI:10.1016/j.gloplacha.2010.03.001.

Wu T, Zhao L, Li R, Wang Q, Xie C, Pang Q. 2013. Recent ground surface warming and its effects on permafrost on the central Qinghai-Tibet Plateau. *International Journal of Climatology* **33**: 920–930. DOI:10.1002/joc.3479.

Xiao Y, Zhao L, Dai YJ, Li R, Pang QQ. 2012. Representing Permafrost Properties in CoLM for the Qinghai-Xizang (Tibetan) Plateau. *Cold Regions Science and Technology* **87**: 68–77. DOI:10.1016/j.coldregions.2012.12.004.

Xue BL, Wang L, Yang K, Tian L, Qin J, Chen YY, Zhao L, Ma YM, Koike T, Hu ZY, Li XP. 2013. Modeling the land surface water and energy cycles of a mesoscale watershed in the central Tibetan Plateau during summer with a distributed hydrological model. *Journal of Geophysical Research-Atmospheres* **118**: 8857–8868. DOI:10.1002/jgrd.50696.

Yang K, Koike T, Ye BS, Bastidas L. 2005. Inverse analysis of the role of soil vertical heterogeneity in controlling surface soil state and energy partition. *Journal of Geophysical Research* **110**: D08101. DOI: 10.1029/2004jd005500

Yang K, Chen YY, Qin J. 2009. Some practical notes on the land surface modeling in the Tibetan Plateau. *Hydrology and Earth System Sciences* **13**: 687–701. DOI:10.5194/hessd-6-1291-2009.

Yang K, He J, Tang WJ, Qin J, Cheng CCK. 2010. On downward shortwave and longwave radiations over high altitude regions: Observation and modeling in the Tibetan Plateau. *Agricultural and Forest Meteorology* **150**: 38–46.

Yao JM, Zhao L, Ding YJ, Gu LL, Jiao KQ, Qiao YP, Wang YX. 2008. The surface energy budget and evapotranspiration in the Tanggula region on the Tibetan Plateau. *Cold Regions Science and Technology* **52**: 326–340.

Yu QH, Roth K, Jin HJ, Pan XC, Schiwek PM, Sheng Y, Wei Z, Wu JC. 2006. Progress of the Sino-German Joint Researches on the Degradation of Permafrost on the Tibetan Plateau. *Journal of Glaciology and Geocryology* **28**: 844–849 (in Chinese with English abstract).

Zeng XB, Wang Z, Wang AH. 2012. Surface Skin Temperature and the Interplay between Sensible and Ground Heat Fluxes over Arid Regions. *Journal of Hydrometeorology* **13**: 1359–1370.

Zhao L. 2009. Proposal for investigation of permafrost and its environment over the Qinghai-Xizang (Tibet) Plateau (ed) (in Chinese with English abstract). Cold and Arid Regions Environmental and Engineering Research Institute, Chinese Academy of Sciences, 47.

Zhao L, Cheng GD, Li SX. 2000. Thawing and freezing processes of active layer in Wudaoliang region of Tibetan Plateau. *Chinese Science Bulletin* **45**: 1205–1211 (in Chinese).

Zhao L, Sheng Y, Xiao Y, Wu TH, Pang QQ, Chen J, Wu JC. 2012. Status of permafrost distribution and thermal dynamics on the Qinghai-Xizang (Tibet) Plateau, China. Abstract C51E-06 presented at 2012 Fall Meeting, AGU: San Francisco, California, 3–7 December.

Zhou YW, Guo DX, Qiu GQ, Cheng GD. 2000. *Geocryology in China*. Science Press: Beijing, China (in Chinese).

Zilitinkevich SS. 1995. Non-local turbulent transport: Pollution dispersion aspects of coherent structure of convective flows. In *Air Pollution Theory and Simulation*, Power H, Moussiopoulos N, Brebbia C (eds). Computational Mechanics Publications: Southampton, Boston; 53–60.